MraY–antibiotic complex reveals details of tunicamycin mode of action

Jonna K Hakulinen[1,3], Jenny Hering[1,2], Gisela Brändén[2], Hongming Chen[1], Arjan Snijder[1], Margareta Ek[1]* & Patrik Johansson[1]*

The rapid increase of antibiotic resistance has created an urgent need to develop novel antimicrobial agents. Here we describe the crystal structure of the promising bacterial target phospho-*N*-acetylmuramoyl–pentapeptide translocase (MraY) in complex with the nucleoside antibiotic tunicamycin. The structure not only reveals the mode of action of several related natural-product antibiotics but also gives an indication on the binding mode of the MraY UDP–MurNAc–pentapeptide and undecaprenyl-phosphate substrates.

Phospho-*N*-acetylmuramoyl-pentapeptide translocase (MraY) is an essential transmembrane enzyme in the bacterial peptidoglycan synthesis pathway[1] and a promising target for developing novel antibiotics. MraY catalyzes the transfer of phospho-*N*-acetylmuramoyl-pentapeptide (p-MurNAc-pp) from UDP–MurNAc-pentapeptide to the carrier lipid undecaprenyl phosphate ($C_{55}P$), forming the products lipid I and uridine monophosphate (UMP) in an Mg^{2+}-dependent reaction[2,3]. MraY belongs to the polyisoprenyl-phosphate *N*-acetylglucosaminosugar-1-phosphate-transferase (PNPT) superfamily of prokaryotic and eukaryotic prenyl sugar transferases[4]. The bacterial PNPT superfamily members synthesize polyprenyl-linked monosaccharides in cell wall assembly[5,6], whereas the eukaryotic members catalyze post-translational glycosylation[7]. MraY is the target of four classes of natural-product nucleoside antibiotics: tunicamycins, ribosamino-uridines, uridylpeptides and capuramycins[8]. Tunicamycin is a widely used tool compound for blocking eukaryotic N-linked glycosylation by inhibiting the UDP–*N*-acetylglucosamine (GlcNAc):dolichol phosphate GlcNAc-1-phosphate transferases (GPTs) that catalyze the transfer of GlcNAc to dolichol phosphate. Tunicamycin has been observed to compete with the sugar substrates of both MraY and GPT, but not with the lipid substrates of the two enzymes[9–13].

Only limited information is available on the detailed structure of the PNPT superfamily and the mechanism behind tunicamycin MraY and GPT inhibition. The first insight into the molecular details of this class of enzymes came with the apo structure of MraY from the non-pathogenic Gram-negative bacterium *Aquifex aeolicus* (AaMraY)[14] and was recently extended with an AaMraY structure in complex with muraymycin D2 (MD2) (ref. 15). To investigate the detailed active site structure of the PNPT family and the molecular basis of tunicamycin binding, MraY from the pathogenic Gram-positive bacterium *Clostridium bolteae* (CbMraY) was expressed in *Escherichia coli* and purified in decylmaltoside (**Supplementary Results**, **Supplementary Fig. 1**). The enzymatic activity of CbMraY and the inhibitory effect of tunicamycin were confirmed using a fluorescence resonance energy transfer (FRET)-based assay[16] (**Supplementary Fig. 1c,d**). CbMraY crystallized as a

dimer in space group $C222_1$ with one molecule in the asymmetric unit. This is in line with AaMraY[14,15] that was found to form a dimer in membrane and in detergent solution as well as in crystals. The sequence identity between *C. bolteae* and *A. aeolicus* MraY is 34%, and they share a similar overall fold of ten transmembrane helices, five cytoplasmic loops and four extracellular loops (**Fig. 1a**). Helix 9 is broken into two segments by a highly conserved glycine residue (G258), which causes the second half to protrude into the lipid bilayer. In contrast to the AaMraY apo structure, but similarly to the recently published AaMraY MD2 complex, CbMraY was found to feature an additional 11-residue helix in between α9b and α10, here denoted as 9c (**Supplementary Figs. 2** and **3**). The amphiphilic 9c helix forms one side of a cytoplasmic cleft lined by loops 5–6 and 7–8 and helices 5–10, composing the active site of the enzyme.

A bound tunicamycin molecule was found in the wide cytoplasmic cavity, interacting with the side chains of F173, G176, N221, F228, N172, D175, D178, D231, H290 and H291 (**Fig. 1**; **Supplementary Fig. 4**). The latter six residues have been shown to be key for MraY activity in previous mutational studies[17], as also confirmed by the low activity of the CbMraY D175N, D231A and H290N mutants (**Supplementary Fig. 5**; **Supplementary Table 1**). Six additional point mutations, L112S, G166F, N221A, F228A, A287N and A287Q were introduced to further investigate the CbMraY active site and the potential entry path of the lipid substrate.

The tunicamycin *N*-acetyl-D-glucosamine ring was found to stack against F173 and P288. This locates the 6′′ hydroxyl group close to the F173 backbone carbonyl and to H290, and places the 4′′ hydroxyl group close to H291 (**Fig. 1**; **Supplementary Fig. 4**). The tunicamine sugar stretches toward the catalytic aspartate cluster with the 9′ hydroxyl group interacting with D231. The conformation of the tunicamine linker with the 5′ hydroxyl group relatively exposed is consistent with the 5′ substitutions of several related nucleosides, including muraymycin. The tunicamycin uracil ring was found to wedge into a small cavity formed by G176, N221 and F228, where N221 interacts with the 4-carbonyl and D178 interacts with the 3-nitrogen of the uracil (**Fig. 1d**; **Supplementary Fig. 4**). Mutating N221 or F228 leads to almost complete inactivation of CbMraY (**Supplementary Fig. 5**; **Supplementary Table 1**), suggesting that these residues are also important for substrate binding, although an N221A mutant in *Bacillus subtilis* MraY (BsMraY) was found to be active[17]. The position of the uracil ring places the 2-carbonyl close to a strong $4\sigma\ F_o - F_c$ peak coordinated by D178 and E300, discussed below. Both these residues are strictly conserved throughout the MraYs and were shown to be important for BsMraY activity[17]. The tunicamycin fatty acyl tail could not be observed in
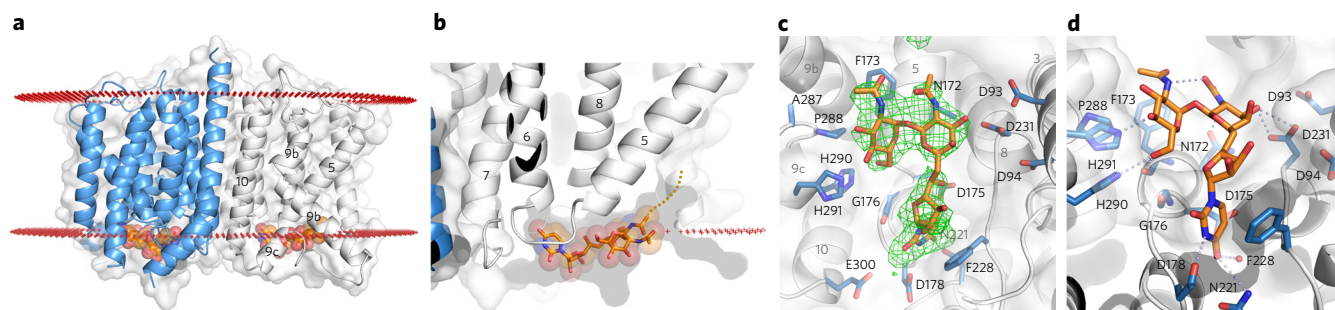
Figure 1 | The MraY tunicamycin complex structure. (**a**) Overview of the CbMraY dimer. (**b**) The bound tunicamycin (orange) in the MraY cytoplasmic cavity. A dashed line indicates the tunicamycin fatty acid tail position. (**c**) Tunicamycin $F_o – F_c$ density contoured at 3.0 σ and a 3-Å carve. (**d**) The MraY uracil pocket. Blue dashes indicate close polar tunicamycin contacts.

the electron density, potentially because of its flexibility and the natural variation of the acyl chain length. However, the side chain of N172 was found to coordinate the fatty acid amide, indicating the direction of the lipid stretching up along helix 5 into the bilayer (**Figs. 1b** and **2b**).

The CbMraY tunicamycin and the AaMraY MD2 complexes[15] both feature a similar active site geometry, in stark contrast to the previously published AaMraY apo structure[14] (**Supplementary Figs. 2** and **3**). Tunicamycin and MD2 share a partly overlapping binding mode with the common uracil motif wedged into the small G176–F228 pocket (AaMraY G194–F262). However, in contrast to tunicamycin, MD2 does not interact with several of the catalytically important residues, including the D93, D94, D231 triad (AaMraY D117, D118, D265) crucial for the MraY transfer reaction[14,17] (**Fig. 2a**). The primary amine of AaMraY K70 is positioned to interact with the MD2 uracil, overlapping with the strong positive CbMraY density close to E300 and D178. Although the CbMraY G33–Q48 peptide stretch could not be reliably modeled, this indicates that the density peak belongs to the corresponding CbMraY K47. The strictly conserved K47 might thus be responsible for coordinating the 2-carbonyl not only of tunicamycin but also of the MraY UDP–MurNAc-pentapeptide substrate, as supported by the low activity of the corresponding *B. subtilis* mutant enzyme[17]. While the tunicamine sugar of the CbMraY complex stretches toward the catalytic aspartates and interacts with D231, the MD2 is split in two arms; The MD2 5′-aminoribosyl protrudes toward loop 7–8 to form an interaction with T52 and G230 (AaMraY T75 and G264), shifting the M229–D231 (AaMraY M263–D265) backbone about 2 Å compared to the tunicamycin-bound structure. The MD2 peptide in turn extends over helix 9c, interacting with the backbone carbonyl of A287 (AaMraY A321) and with the side chain of Q271 (AaMraY Q305). The peptidic moiety partly occupies the same volume as the tunicamycin GlcNAc. This places the lipid attachment point of the muraymycin-type inhibitors close to the 2″ amide of tunicamycin, about 5 Å away from the tunicamycin fatty acid in the large cavity formed by helices 4, 5 and 9 (**Fig. 2b**).

The strong sequence conservation suggests that the active site geometry is retained throughout the MraY family (**Supplementary Fig. 6a**). To get a better understanding of substrate binding of these enzymes, UDP–GlcNAc and UDP–MurNAc L-Ala were docked into the active site of CbMraY (**Supplementary Fig. 7**). The uracil and ribose motifs of UDP–GlcNAc are likely to bind in a similar manner as tunicamycin. This locates the diphosphate group close to the catalytic residues D93, D94 and K111 (ref. 18) and D231 involved in Mg^{2+} ion binding[15]. The *N*-GlcNAc ring partially overlaps with the tunicamycin counterpart, while the position of the L-Ala indicates the direction of the substrate pentapeptide, interacting with helix 9c and the neighboring loops, similarly to the MD2

peptide (**Supplementary Fig. 7b**). This conformation is supported by the fact that replacing A287, positioned at the N-terminal end of helix 9c by bulkier residues, such as asparagine, reduces enzymatic activity significantly (**Supplementary Figs. 5** and **7**; **Supplementary Table 1**). Previous studies have also indicated that these segments are involved in sugar substrate recognition in many of the bacterial PNPTs[6]. On the basis of the tunicamycin fatty acid chain position, the muraymycin lipid attachment point and the substrate phosphate-group position, it seems likely that the $C_{55}P$ lipid substrate would enter the active site along the shallow cleft of α5. This theory is further strengthened by the observed low activity of the L112S and G166F mutants, located in helices 4 and 5 (**Supplementary Fig. 5**; **Supplementary Table 1**). L112 is conserved as a hydrophobic and/or large residue in MraYs, while G166 is conserved as a small residue, suggesting that the shape and properties of this region are important for activity. An entry path of the $C_{55}P$ between helices 4, 5 and 9 is complicated by the reported lack of lipid competitivity of tunicamycin[12], but would be in line with the one-step MraY mechanism in which D93 deprotonates one of the $C_{55}P$ hydroxyls that makes a nucleophilic attack on the β-phosphate of UDP–MurNAc to form the lipid I product[17,18].

To obtain some insight into the basis of tunicamycin cross-reactivity with the eukaryotic GPT enzymes, the human GPT (HuGPT) sequence was compared to the CbMraY structure and a number of related sequences (**Supplementary Fig. 6a**). The D93, D94, D231 and N172 cluster of CbMraY is well conserved
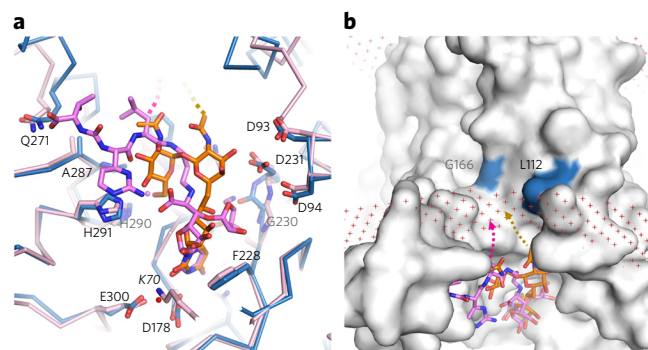

Figure 2 | Comparison of tunicamycin and MD2 binding. (**a**) Superposition of the CbMraY tunicamycin (blue/orange) and AaMraY MD2 structures (magenta, PDB ID 5CKR). The side chain of AaMraY K70 is indicated in italics (bottom). (**b**) Surface representation of the potential CbMraY $C_{55}P$ binding cleft. Dashed lines indicate the tunicamycin and muraymycin lipid tail locations. Positions of L112 and G166 are indicated in blue.

in the GPT enzymes. D175 is replaced by an alanine in the GPTs, but G176, N221 and F228 are conserved. The sequence conservation indicates some similarity between the MraY and GPT core active sites. However, the helix 9–10 stretch of HuGPT significantly differs from the MraY sequences, with no convincing equivalent to the CbMraY H290–H291 dyad. The differences in this segment as well as in the N terminus of helix 2 and the C terminus of helix 3 indicate areas where selectivity between the bacterial and eukaryotic enzymes could potentially be exploited to reduce the toxicity of new MraY inhibitors (**Supplementary Fig. 6b**).

The difficulties associated with chemical synthesis of many natural-product antibiotics have limited their potential as leads for drug discovery. However, the full synthesis of tunicamycin[19,20] was recently further developed to enable the production of a variety of tunicamycin analogs[21]. In addition, the *Streptomyces* pathway for tunicamycin biosynthesis was recently elucidated[22]. These breakthroughs will, together with the MraY tunicamycin complex presented, dramatically enhance the potential for further development of the nucleoside antibiotics as means to combat bacterial infections.

Methods

Methods, including statements of data availability and any associated accession codes and references, are available in the online version of the paper.

Accession codes. Atomic coordinates and structure factors for the reported crystal structure have been deposited with the Protein Data Bank under accession code 5JNQ.

References

1. Boyle, D.S. & Donachie, W.D. *J. Bacteriol.* **180**, 6429–6432 (1998).
2. Anderson, J.S., Matsuhashi, M., Haskin, M.A. & Strominger, J.L. *Proc. Natl. Acad. Sci. USA* **53**, 881–889 (1965).
3. Struve, W.G. & Neuhaus, F.C. *Biochem. Biophys. Res. Commun.* **18**, 6–12 (1965).
4. Lehrman, M.A. *Glycobiology* **4**, 768–771 (1994).
5. Lehrman, M.A. *Glycobiology* **1**, 553–562 (1991).
6. Anderson, M.S., Eveland, S.S. & Price, N.P. *FEMS Microbiol. Lett.* **191**, 169–175 (2000).
7. Heifetz, A. & Elbein, A.D. *J. Biol. Chem.* **252**, 3057–3063 (1977).
8. Dini, C. *Curr. Top. Med. Chem.* **5**, 1221–1236 (2005).
9. Tkacz, J.S. & Lampen, O. *Biochem. Biophys. Res. Commun.* **65**, 248–257 (1975).
10. Tamura, G., Sasaki, T., Matsuhashi, M., Takatsuki, A. & Yamasaki, M. *Agric. Biol. Chem.* **40**, 447–449 (1976).
11. Schwarz, R.T. & Datema, R. *Trends Biochem. Sci.* **5**, 65–67 (1980).
12. Brandish, P.E. *et al. Antimicrob. Agents Chemother.* **40**, 1640–1644 (1996).
13. Keller, R.K., Adair, W.L. Jr. & Ness, G.C. *J. Biol. Chem.* **254**, 9966–9969 (1979).
14. Chung, B.C. *et al. Science* **341**, 1012–1016 (2013).
15. Chung, B.C. *et al. Nature* **533**, 557–560 (2016).
16. Shapiro, A.B., Jahić, H., Gao, N., Hajec, L. & Rivin, O. *J. Biomol. Screen.* **17**, 662–672 (2012).
17. Al-Dabbagh, B. *et al. Biochemistry* **47**, 8919–8928 (2008).
18. Al-Dabbagh, B. *et al. Biochimie* **127**, 249–257 (2016).
19. Suami, T., Sasai, H., Matsuno, K. & Suzuki, N. *Carbohydr. Res.* **143**, 85–96 (1985).
20. Myers, A.G., Gin, D.Y. & Rogers, D.H. *J. Am. Chem. Soc.* **116**, 4697–4718 (1994).
21. Li, J. & Yu, B. *Angew. Chem. Int. Edn Engl.* **54**, 6618–6621 (2015).
22. Wyszynski, F.J. *et al. Nat. Chem.* **4**, 539–546 (2012).

Acknowledgments

Author contributions

A.S. and M.E. designed the study, J.K.H. established purification and crystallized the protein, J.H. collected and analyzed the activity data, J.K.H. and P.J. collected the crystallographic data, P.J. solved and built the initial model, P.J. and G.B. refined the structure, H.C. performed the docking studies, J.K.H., G.B., M.E. and P.J. prepared the manuscript with input from all authors.

Competing financial interests

The authors declare competing financial interests: details accompany the online version of the paper.

Additional information

Any supplementary information, chemical compound information and source data are available in the online version of the paper. Reprints and permissions information is available online at http://www.nature.com/reprints/index.html. Correspondence and requests for materials should be addressed to P.J. or M.E.

ONLINE METHODS

Expression and purification of *Clostridium bolteae* MraY. In a previous study, 24 MraY orthologs were screened for expression levels and stability[23]. The most promising orthologs from *Clostridium bolteae, Bacillus subtilis* and *Thermus thermophilus* were scaled up for further characterization. CbMraY had the highest expression yield and adequate biochemical properties for crystallization. The CbMraY construct used for crystallization included an N-terminal PelB signal sequence, a TEV cleavable N-terminal split GFP sequence and a C-terminal His$_{10}$ tag in the pET26b$^+$ plasmid[23]. CbMraY was overproduced in *Escherichia coli* BL21(gold)DE3 cells in ZY505 medium[24] with 0.1 mg/ml kanamycin and antifoam in a fermenter with 40% dissolved oxygen. Cells were grown to optical density at 600 nm(OD$_{600}$) = 0.4–0.5 at 37 °C. Protein expression was induced with 0.1 mM isopropyl thiogalactoside (IPTG) at 19 °C for 17–18 h. All steps in membrane preparation and protein purification were carried out at 4 °C. Harvested cells were resuspended in 25 mM HEPES pH 7.5, 150 mM NaCl, 10% (v/v) glycerol, 1 mM MgCl$_2$, 0.1 mg/ml lysozyme, 1 mM TCEP, 1 mM PMSF, cOmplete protease inhibitor (Roche) and 0.3 μl/ml benzonase (Sigma). Cells were lysed in a constant system cell disruptor at 28 kpsi and the cell debris was removed by centrifugation at 4,900 × g for 15 min. The membranes were isolated by ultracentrifugation at 138,000 × g for 60 min and resuspended in membrane buffer containing 40 mM HEPES pH 7.5, 300 mM NaCl, 1 mM TCEP, 10% (v/v) glycerol, 1 mM PMSF, cOmplete protease inhibitor. CbMraY was solubilized in 25 mM decylmaltoside (DM) for 2 h. Insoluble material was separated by ultracentrifugation at 220,000 × g for 25 min. The solubilized fraction was diluted 1:1 in membrane buffer and adjusted to pH 8.0 using 10 M NaOH. CbMraY was bound to cobalt TALON resin in batch mode for 60 min and washed with 10 column volumes (CV) 20 mM HEPES pH 8.0, 300 mM NaCl, 5 mM DM, 1 mM TCEP, 10 mM imidazole, 10% (v/v) glycerol, 1 mM PMSF, cOmplete. To separate contaminating DnaK chaperone and FtsH protease from CbMraY, the resin was washed with 7.5 CV 20 mM HEPES pH 8.0, 300 mM KCl, 5 mM DM, 1 mM TCEP, 30% (v/v) glycerol, 30 mM imidazole, 1 mM PMSF, 8 mM ATP, 10 mM MgCl$_2$, cOmplete and with 7.5 CV, 20 mM HEPES pH 7.5, 300 mM KCl, 3 mM DM, 1 mM TCEP, 30 mM imidazole, 1 mM PMSF, 8 mM ATP, 10 mM MgCl$_2$. In a further wash step the buffer was changed to 20 mM HEPES pH 7.5, 150 mM NaCl, 3 mM DM, 1 mM TCEP, 30 mM imidazole, 0.1 mM PMSF and CbMraY was eluted in the same buffer with 140 mM imidazole. 20 μM tunicamycin (Santa Cruz Biotechnology) was added to the eluate and incubated at 4 °C for 60 min. Subsequently, the protein was concentrated using an Amicon spin concentrator with a 50 kDa cutoff. Size-exclusion chromatography was carried out using a Superdex 200 10/30 column (GE Healthcare) in a mobile phase of 20 mM HEPES pH 7.5, 150 mM NaCl, 3 mM DM, 1 mM TCEP and 20 μM tunicamycin.

Expression of CbMraY wild-type and mutant proteins for activity measurements. CbMraY proteins were overproduced in *E. coli* BL21(gold)DE3 cells in SB medium as 100-ml cultures with 0.1 mg/ml kanamycin in flasks. Cells were grown to OD$_{600}$ = 0.4–0.5 at 37 °C and 210 r.p.m. Protein expression was induced with 0.1 mM IPTG at 19 °C for 17–18 h. Cell disruption and membrane preparation were performed as described above. Equal expression levels of the MraY proteins were verified by western blot. Total membrane protein concentration was determined via Bradford assay (Novexin Bradford ULTRA kit) using a BSA standard curve.

Activity measurement. Activity of CbMraY was investigated using a previously published FRET-based assay[16]. Briefly, the assay was performed in 384-well black polystyrene assay plates in a total volume of 9 μl. An assay buffer containing 50 mM Tris–HCl pH 7.5, 0.5 M trehalose, 150 mM KCl, 50 mM MgCl$_2$, 1 mM DTT, and 0.05% Triton X-100 was used. *E. coli* membranes containing overexpressed CbMraY were incubated with 20 μM undecaprenyl phosphate (C$_{55}$P) and 24 μM 1,2-dipalmitoyl-sn-glycero-3-phosphoethanolamine-*N*-(lissamine rhodamine B sulfonyl) (LRPE) in assay buffer for 30 min. The reaction was initiated with 2 μM UDP–MurNAc-L-Ala-γ-D-Glu-*m*-DAP-D-Ala-D-Ala labeled with BODIPY–FL–sulfosuccinimidyl ester (B-UNAM-pp) and 0 mM or 5 mM uridine 5′-monophosphate (UMP). Fluorescence was excited at 485 nm and detected simultaneously at 520 nm and 590 nm every minute for 30 min in a PheraStar plate reader (BMG Labtech, Cary, NC).

Triplicate wells were averaged and progress curves from inhibited reactions with 5 mM UMP were subtracted from uninhibited progress curves (0 mM UMP). The reactions were run under initial velocity conditions. 5 μg/ml total membrane protein concentration of the wild type was used to perform linear progress curves throughout the 30 min reaction. Since the rate is directly proportional to the enzyme concentration, the total membrane protein concentrations of the mutant proteins were adjusted to obtain similar initial rates as for the wild type. Initial rates were calculated from the change in ΔF520 nm (inhibited reaction progress curves with 5 mM UMP subtracted from uninhibited reaction progress curves) for the first 2 min of the reactions by using a linear fit. For inhibition experiments, tunicamycin was diluted from a 1 mM stock solution in DMSO with assay buffer. 20 μg of *E. coli* membranes containing overexpressed CbMraY were incubated with 125 μM tunicamycin, 10 μM C$_{55}$P and 16 μM LRPE in assay buffer for 30 min before initiating the reaction with 0.1 μM B-UNAM-pp. Reactions without tunicamycin, but with DMSO were used as controls to verify the activity of MraY. Data were analyzed with MATLAB and Statistics Toolbox Release 2013b (The MathWorks Inc.).

Crystallization, data collection and refinement of *C. bolteae* MraY. Initial hits for the CbMraY–tunicamycin complex crystals were obtained in the Memgold2 screen (Molecular Dimensions) 100 mM Hepes pH 7.5 and 33% PEG 400 condition. The crystallization condition was further optimized using a commercial additive screen (Hampton Research) and the best hits were obtained using 4% acetone. CbMraY was finally crystallized at a concentration of 7 mg/ml together with 100 μM tunicamycin in 15–23 % (v/v) PEG 400, 100 mM HEPES pH 7.5–8.25, 4 % (v/v) acetone in hanging drops at 20 °C. The crystals were grown as thin plates and harvested in 7–14 d. Data was collected at beamlines I24 (DIAMOND, UK) and beamlines ID23-1 and ID29 (ESRF, France). Because of the heterogeneity in the crystal packing, X-ray mesh screening was used to identify the most ordered regions of each sample[25]. A first data set was collected and processed to a resolution of 2.9 Å in the a* and b* directions and 3.9 Å in the c* direction using XDS[26]. The crystal was found to belong to space group C222$_1$ with cell dimensions of 92.8 105.4 134.9 Å, indicating one or two molecules in the asymmetric unit, corresponding to a solvent content of 72 and 44%, respectively. Molecular replacement in PHASER[27] using a set of mosaic models of the *Aquifex aeolicus* MraY structure[14] (PDB 4J72) did not result in any clear solutions. However, manual inspection indicated that one of the runs with a TFZ score of 5.4 packed to form a dimeric structure across a crystallographic two-fold axis. The initial phases of this crude solution were significantly improved by solvent flattening and histogram matching in DM[28] and statistical density modification in Parrot[29]. To increase the radius of convergence, a brute force script combining Parrot density modification with cycles of phase restrained chain tracing using Buccaneer in build-only mode[30] followed by refinement in Buster (Global Phasing Ltd, Cambridge United Kingdom, version 2.11.6) was used. Regions of weak 2F$_o$ − F$_c$ density were filtered out, and promising models were used as starting points for new sets of runs. In order to reduce bias, crystals were soaked in a number of heavy atom salts and a data set of crystals soaked in 1 mM K$_2$Pt(NO$_2$)$_4$ was collected to 3.9 Å close to the platinum L-III edge. The HLA coefficients of the best CbMraY model were used by SHARP[31] to locate a single platinum site in the anomalous and isomorphous log likelihood gradient maps. Subsequent density modification and extensive phase-restrained build–refine cycles intervened by manual rebuilding resulted in an R$_{free}$ of 32%. During the course of the refinement, a second high-resolution native data set was obtained, improving the resolution to 2.6 Å in the a* and b* and 3.9 Å in the c* direction, using a CC1/2 = 0.5 cutoff. The data was analyzed by the UCLA Diffraction Anisotropy Server (http://services.mbi.ucla.edu/anisoscale/) (**Supplementary Fig. 8**) and STARANISO (http://staraniso.globalphasing.org) and subjected to further refine cycles using Buster combined with manual rebuilding in Coot[32]. Tunicamycin was fitted to a strong 7σ F$_o$ − F$_c$ density found in the MraY cytoplasmic cavity using Flynn (OpenEye, Santa Fe, NM) (**Fig. 1c**) and refined. Most of the tunicamycin fatty acid chain could not be reliably traced and was omitted. The refinement rendered a final MraY model with an R/R$_{free}$ of 0.226/0.252 and 98.7% of the side chains within accepted Ramachandran regions. Full data collection and refinement statistics can be found in **Supplementary Table 2**.

Molecular modeling. A putative MraY catalytic model was constructed by combing the CbMraY structure and the previously reported AaMraY apo structure (PDB 4J72); The AaMraY apo and the CbMraY tunicamycin complex were aligned by using Maestro (Schrodinger Inc., release 2016.01) and the magnesium ion was added to the empty tunicamycin complex. The resulting structure was subsequently subjected to backbone-constrained minimization. A template guided docking protocol was used to generate binding poses for UDP–GlcNAc via a multiple-step procedure. First the initial 3D conformation of UDP–GlcNAc was created from 2D SMILES strings by using Corina[33] (version 3.6) and further optimized in Maestro with the OPLS3 force field. Second, the optimized UDP–GlcNAc conformer was superimposed onto the bound conformation of tunicamycin in the CbMraY structure using MOE (Chemical Computing Group Inc., release 2015.10) and the aligned UDP–GlcNAc conformation was used as a starting point, going through a constrained conformational search using the conformational search module in Maestro software, in which the atoms in the uracil and ribose motifs were fixed and remaining atoms were allowed to move freely to sample low-energy conformers. Third, after the constrained conformation search, a set of 140 low-energy conformers of UDP–GlcNAc, in which the uracil and ribose rings were kept close to the observed tunicamycin conformation, were collected as input structures for docking into the prepared MraY catalytic protein model. The structures were docked into the model using the Glide module of Maestro in refinement mode. Docking was thus done using the ligands' starting conformations

without conformational and positional sampling. 140 docking poses of UDP–GlcNAc were monitored and a single best conformation from a cluster of related poses was selected. The selected pose was merged with the catalytic protein model to form a complex structure and was subjected to energy minimization constraining the protein backbone atoms. The binding mode for UDP–MurNAc L-Ala was generated via a similar protocol.

23. Backmark, A.E. *et al. Protein Sci.* **22**, 1124–1132 (2013).
24. Studier, F.W. *Protein Expr. Purif.* **41**, 207–234 (2005).
25. Bowler, M.W. *et al. Acta Crystallogr. D Biol. Crystallogr.* **66**, 855–864 (2010).
26. Kabsch, W. *Acta Crystallogr. D Biol. Crystallogr.* **66**, 125–132 (2010).
27. McCoy, A.J. *et al. J. Appl. Crystallogr.* **40**, 658–674 (2007).
28. Cowtan, K., Zhang, K.Y.J. & Main, P. *International Tables for Crystallography, Crystallography of Biological Macromolecules* (Kluwer Academic Publishers, 2001).
29. Cowtan, K. *Acta Crystallogr. D Biol. Crystallogr.* **66**, 470–478 (2010).
30. Cowtan, K. *Acta Crystallogr. D Biol. Crystallogr.* **64**, 83–89 (2008).
31. de La Fortelle, E. & Bricogne, G. *Methods Enzymol.* **276**, 472–494 (1997).
32. Emsley, P. & Cowtan, K. *Acta Crystallogr. D Biol. Crystallogr.* **60**, 2126–2132 (2004).
33. Gasteiger, J., Rudolph, C. & Sadowski, J. *Tetrahedron Comp. Method.* **3**, 537–547 (1990).